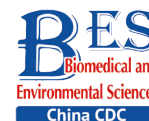


## Original Article



## Identifying Comprehensive Genomic Alterations and Potential Neoantigens for Cervical Cancer Immunotherapy in a Cohort of Chinese Squamous Cell Carcinoma of the Cervix

Meng Wu<sup>1,2</sup>, Jialu Zhou<sup>3</sup>, Zhe Zhang<sup>4,#</sup>, and Yuanguang Meng<sup>2,3,#</sup>

1. School of Medicine, Nankai University, Tianjin 300071, China; 2. Department of Obstetrics and Gynecology, The First Medical Center of Chinese PLA General Hospital, Beijing 100853, China; 3. Department of Obstetrics and Gynecology, Chinese PLA Medical School, Beijing 100853, China; 4. Department of Obstetrics and Gynecology, The Seventh Medical Center of Chinese PLA General Hospital, Beijing 100700, China

### Abstract

**Objective** Genomic alterations and potential neoantigens for cervical cancer immunotherapy were identified in a cohort of Chinese patients with cervical squamous cell carcinoma (CSCC).

**Methods** Whole-exome sequencing was used to identify genomic alterations and potential neoantigens for CSCC immunotherapy. RNA Sequencing was performed to analyze neoantigen expression.

**Results** Systematic bioinformatics analysis showed that C>T/G>A transitions/transversions were dominant in CSCCs. Missense mutations were the most frequent types of somatic mutation in the coding sequence regions. Mutational signature analysis detected signature 2, signature 6, and signature 7 in CSCC samples. *PIK3CA*, *FBXW7*, and *BICRA* were identified as potential driver genes, with *BICRA* as a newly reported gene. Genomic variation profiling identified 4,960 potential neoantigens, of which 114 were listed in two neoantigen-related databases.

**Conclusion** The present findings contribute to our understanding of the genomic characteristics of CSCC and provide a foundation for the development of new biotechnology methods for individualized immunotherapy in CSCC.

**Key words:** Cervical squamous cell carcinoma; Genome alteration; Neoantigens; Immunotherapy

*Biomed Environ Sci*, 2024; 37(6): 565-580 doi: [10.3967/bes2024.064](https://doi.org/10.3967/bes2024.064)

ISSN: 0895-3988

[www.besjournal.com](http://www.besjournal.com) (full text)

CN: 11-2816/Q

Copyright ©2024 by China CDC

### INTRODUCTION

Cervical cancer (CC) is one of the most common gynecological malignancies; approximately 604,127 new cases were reported worldwide in 2020, of which nearly 85% occurred in low- and middle-income countries<sup>[1,2]</sup>. In China, the mortality rate of CC in 2022 was as high as 55.07%<sup>[3]</sup>. Cervical squamous cell carcinoma (CSCC) accounts for approximately 70% of all CCs worldwide, which is significantly higher than the rate of cervical adenocarcinoma<sup>[4]</sup>. Although surgery is an

effective treatment for early-stage CC, 20%–30% of CC patients in advanced stages experience recurrence or distant metastasis after chemotherapy administered concurrently with radiation therapy, and the 5-year survival rate is only 5%–15%<sup>[5]</sup>. A comprehensive description of the genomic and molecular characteristics of 228 primary CCs (including 144 CSCC cases) was reported in The Cancer Genome Atlas (TCGA) research network, although only 18 Asians were included<sup>[6]</sup>. CSCC remains a disease with high morbidity and mortality in China, and the number of sequencing samples

<sup>#</sup>Correspondence should be addressed to Zhe Zhang, PhD, Tel: 86-18810999596, E-mail: [zhangzhe301@126.com](mailto:zhangzhe301@126.com); Yuanguang Meng, Professor, PhD, Tel: 86-13501093681, E-mail: [meng6512@vip.sina.com](mailto:meng6512@vip.sina.com)

Biographical note of the first author: Meng Wu, female, born in 1992, MD, majoring in obstetrics and gynecology.

available for evaluating genomic alterations in CSCC is small. Therefore, it is necessary to establish a comprehensive genetic profile of the Chinese population with a larger sample size through next-generation sequencing.

Most CSCCs are caused by high-risk subtypes of human papillomavirus (HPV), and the disease could therefore be prevented through well-established screening and vaccination programs<sup>[7]</sup>. However, the prevalence and mortality of CSCC have remained relatively high because of low vaccination rates. In addition to increasing the rate of vaccination, the development of new treatments for CSCC is critical. In recent years, immunotherapy has emerged as a potentially effective therapeutic approach. Immune checkpoint inhibitors (ICIs) have been successfully applied to the treatment of different types of cancer, such as gastric, lung, and head and neck cancer, which has significantly prolonged the survival of patients<sup>[8-10]</sup>. Pembrolizumab was the first Food and Drug Administration (FDA)-approved first-line immunotherapy for CC; however, it showed positive results in a minority of CC patients<sup>[11]</sup>. In addition to ICIs, several immunotherapeutic approaches for advanced cervical cancer, including HPV therapeutic vaccines and adoptive cellular therapy, are under study, and promising efficacy data are emerging<sup>[12,13]</sup>.

The genetic instability of tumor cells often leads to numerous somatic mutations, and the expression of non-synonymous mutations generates tumor-specific antigens called neoantigens<sup>[14]</sup>. Neoantigens are presented by human leukocyte antigen (HLA) class I/II molecules and can activate CD8+ and CD4+ T cells, resulting in the induction of immune responses<sup>[15]</sup>. Because neoantigens are not expressed in normal tissues and are highly immunogenic, they have emerged as novel targets for tumor immunotherapy. Extensive analysis of the genomic variations in CC identified a close association with mutated genes such as *PIK3CA*, *FBXW7*, *EP300*, *MLL3*, *CASP8*, and *FADD*<sup>[16]</sup>. However, research aimed at identifying CSCC neoantigens through the analysis of genetic mutations is lacking.

In this study, we explored the genomic characteristics of CSCC using whole-exome sequencing (WES) data and identified potential neoantigens by WES and RNA sequencing (RNA-seq). The present findings improve our understanding of genetic alterations in CSCC and identify relevant neoantigens, which may provide effective immunotherapeutic targets for the treatment of

CSCC.

## MATERIALS AND METHODS

### *Patient Material*

Written informed consent was obtained from each individual before enrollment in the study. Primary tumor tissues and peripheral blood were collected from patients diagnosed with CSCC at the Obstetrics and Gynecology Department of the Chinese Liberation Army General Hospital between January 1, 2021 and May 1, 2022. Sample collection, HPV typing, and pathological examination were performed according to the guidelines or requirements of the patients. Data on clinical characteristics were collected from medical records.

The study included 60 samples from 30 CSCC patients. Twenty-nine surgically resected tumor tissues (4–6 g per sample) were snap-frozen in liquid nitrogen and stored at  $-80^{\circ}\text{C}$ , and one was paraffin-embedded. Additionally, 30 blood samples (3–5 mL per sample) were collected as controls and stored in anticoagulant tubes containing ethylenediaminetetraacetic acid. The blood and anticoagulant were thoroughly mixed and stored at  $-20^{\circ}\text{C}$ . All slides were diagnosed by two experienced pathologists using hematoxylin and eosin (H&E) staining.

### *DNA Extraction and Whole-Exome Sequencing*

Tumor and matched normal DNA were extracted using the TIANamp Genomic DNA Kit (DP304, TIANGEN, Beijing, China) using fresh-frozen tumor tissues and paired blood samples. The QIAamp DNA FFPE Tissue Kit (56404, Qiagen, Hilden, Germany) was used to extract genomic DNA (gDNA) from formalin-fixed paraffin-embedded (FFPE) tissues. To ensure the quality of the gDNA, two methods were employed: (1) Agarose gel electrophoresis to analyze the degree of DNA degradation and contamination; and (2) Qubit® 3.0 Fluorometer (Invitrogen, USA) to quantify the DNA concentration accurately. Finally, DNA samples with a gDNA concentration  $\geq 20$  ng/ $\mu\text{L}$  and a minimum of  $0.4$   $\mu\text{g}$  gDNA per sample were used for library construction.

WES was performed using  $0.4$   $\mu\text{g}$  of gDNA from each sample. Library construction and capture experiments were performed using the Agilent SureSelect Human All Exon V6 Kit (Cat. No. 5190–8864, Agilent Technologies, Santa Clara, CA, USA) following the manufacturer's instructions. During this process, index codes were added to each

sample. The gDNA was fragmented into pieces measuring approximately 180–280 bp using a hydrodynamic shearing system (Covaris, Massachusetts, USA). After end repair, phosphorylation, and A-tailing, adapter oligonucleotides were added to create libraries. High-fidelity polymerase was used to amplify DNA fragments with ligated adaptor molecules on both ends to ensure sufficient library volume. The libraries were then hybridized with a solution of biotin-labeled probes, and exons were captured using streptomycin magnetic beads. In preparation for sequencing, PCR was used to add index tags to the captured libraries. After purification and quantification, the index-encoded samples were clustered using the HiSeq PE Cluster Kit V2.5 (Illumina). The DNA libraries were sequenced on the Illumina HiSeq X-TEN platform (San Diego, CA, USA), generating 150 bp paired-end reads after cluster generation.

### **RNA Extraction and RNA Sequencing**

To create the library, a minimum of 1 µg of total RNA was necessary. RNA was extracted from fresh tumor tissues using the Qiagen RNeasy Mini kit (74106, Qiagen, Germany) and RNA-Seq libraries were prepared using the NEBNext® Ultra™ RNA Library Prep Kit (E7530L, Illumina, USA). The library was quantified using the Qubit2.0 Fluorometer detection kit (Q32866, Invitrogen, USA) and diluted to 1.5 ng/µL. The Agilent 2100 bioanalyzer (2100, Agilent, USA) was used to detect the insert size of the library and accurately determine the effective concentration (higher than 2 nmol/L) to ensure quality. Once the library passed inspection, it was categorized according to the effective concentration and target off-machine data volume. Finally, Illumina sequencing was performed, which generated 150 bp paired-end reads.

### **Sequencing Data Analysis and Variation Identification**

Raw data were preprocessed by Fastp (v.0.23.4, <https://github.com/OpenGene/fastp>) to obtain clean data using the following steps: (1) adapter trimming; (2) removal of reads with > 10% N bases; (3) removal of reads in which > 50% of the length contained low-quality bases (quality threshold < 5); and (4) sliding window trimming, in which the bases with an average quality below the cutoff value (default was 20) in the sliding window (default was 4 bp) were cut. BWA<sup>[17]</sup>, Picard (<http://broadinstitute.github.io/picard/>), and GATK tools<sup>[18]</sup> were used for read

alignment, variant calling, and identification of single-nucleotide variants (SNVs) and small insertions and deletions (InDels). Default parameters were used in all software programs for identifying mutations in matched normal-tumor samples. To further annotate candidate somatic mutations, we used Funcotator (FUNCTIONAL annotATOR)<sup>[19]</sup> and generated mutation annotation format (MAF) files that included position, function, and sequencing data supporting the mutation status.

Somatic copy number alterations (CNAs) were evaluated using the CNVkit<sup>[20]</sup> pipeline (v.0.9.10). The default log<sub>2</sub> threshold was applied to detect copy number gains or losses in target regions. Heatmaps of copy number alterations were obtained by loading the resulting files with segmented copy numbers into Integrative Genomics Viewer (IGV, v.2.15.9)<sup>[21]</sup> for visualization. The GISTIC (Genomic Identification of Significant Targets in Cancer) 2.0 pipeline (v.2.0.23)<sup>[22]</sup> was then applied to detect the significantly amplified and deleted regions with somatic CNAs with FDR (false discovery rate) < 0.20. A confidence level of 0.90 was set to determine significance. The GISTIC2.0 output files were visualized by the R package ggplot2.

Synonymous and nonsynonymous somatic SNVs were analyzed using the R package maftools to identify the type of point mutations in each tumor sample<sup>[23]</sup>. The mutational signature contribution of each tumor sample was estimated using the R package deconstructSigs<sup>[24]</sup>, which accurately reconstructed the mutational profiles of tumor samples by identifying linear combinations of pre-defined features. This tool established the correspondence between the 96 mutation spectrum and the 30 mutational characteristics of the Catalog of Somatic Mutations in Cancer (COSMIC) database. The calculated weights were assigned to the mutational signatures, in which a higher weight indicates a more significant contribution.

Two computational methods, Oncodrive-CLUSTL<sup>[25]</sup> and OncodriveFML<sup>[26]</sup>, were used to detect potential driver genes. The OncodriveCLUSTL algorithm uses a sequence-based clustering technique to identify linear clustering bias in the observed somatic mutations. OncodriveFML is a tool that detects genes under positive selection by analyzing the functional impact bias of the observed somatic mutations. Default values were used for all software parameters, and driver genes were identified according to the following criterion: genes with an FDR < 0.25 in both OncodriveCLUSTL and OncodriveFML were considered as driver genes.

MutSigCV<sup>[27]</sup> was used to perform convolution tests to identify significantly mutated genes (SMGs). This software comprehensively analyzes somatic SNVs and InDels to obtain SMGs whose mutation rate is significantly higher than the background mutation rate. Genes with FDR < 0.20 were considered as SMGs.

RNA-seq raw reads that passed the Illumina RTA quality filter were first preprocessed with Trim Galore (v.0.6.10) to remove adapter sequences and for base quality control. Then, STAR software (v.2.7.10b) was used to align the remaining RNA reads to the NCBI human reference genome (GRCh38). Finally, the number of reads aligning to each gene in the mapping results was calculated as Fragments Per Kilobase per Million (FPKM) values using RSEM software (v.1.3.3).

#### **HLA Typing and Neoantigen Detection**

HLAcan tool (v.2.1.2)<sup>[28]</sup> was used to determine HLA types across the patients' whole-exome sequences by aligning reads to HLA sequences from the international ImMunoGeneTics project/human leukocyte antigen (IMGT/HLA) database. Neoantigen analysis was performed using the NeoPredPipe pipeline<sup>[29]</sup>, which integrates ANNOVAR and netMHCpan to process neoantigens predicted from multi-region Variant Call Format (VCF) files. ANNOVAR correctly annotates variants from VCF files to identify non-synonymous variants, generating peptide sequences based on variant bases. Before executing netMHCpan, HLA haplotypes were cross-referenced with available HLA haplotypes, and epitopes of 8–11 mer length (known to be likely for peptides presented by human MHC class I molecules) were specified to make predictions. NetMHCpan 4.1<sup>[30]</sup> was used to detect the binding affinity strength of each mutant peptide to sample-specific HLA alleles to identify exome-derived neoantigens. Finally, the results were filtered according to half-maximal inhibitory concentration (IC50) and rank value (IC50 < 500 nmol/L and %Rank < 2%). A neoantigen was considered expressed if a mutated gene Tumor-*FPKM* ≥ 0.5 when RNA-seq was available.

#### **Visualization and Statistical Analysis**

All graphical analyses were performed in the R statistical environment (v. 4.2.2). *P*-value calculation methods and multiple testing corrections are reported in the text. Because of the limited sample size, all analyses were conducted at a two-sided significance level of 0.2 (exceptional cases stated

otherwise). Linear correlations were assessed using Pearson's correlation coefficient.

## **RESULTS**

#### **Samples and Clinical Data**

A total of 60 paired samples from patients who had undergone radical hysterectomy without radiotherapy or chemotherapy were analyzed. The samples included 30 primary tumor tissues and 30 matched peripheral blood samples. Of the 30 patients, 22 were HPV-positive, and 8 were HPV-negative ([Supplementary Table S1](#), available in [www.besjournal.com](http://www.besjournal.com)). The patients ranged in age from 24 to 77 years, with an average age of 50.3 years. The clinical stages (International Federation of Gynecology and Obstetrics [FIGO] 2018) of the patients were as follows: 12 in stage I, 12 in stage II, and 6 in stage III. The pathological types of all samples were squamous cell carcinoma with varying levels of differentiation: 6 cases were low, 17 were middle, and 7 were middle-low. Among the patients, 9 had lymph node metastasis, 22 had lymphovascular space involvement, 3 had parametrial invasion, 21 had deep stromal invasion (infiltration depth > 1/2), and 3 had a positive vaginal resection margin. During the follow-up period of 6–19 months (median, 12.5 months), 3 cases (10%) experienced tumor recurrence.

#### **Genomic Alterations**

**SNVs and InDels Analysis** After performing WES on 30 CSCCs and matched control samples (peripheral blood cells) using the Illumina X10 platform (Illumina Inc., San Diego, CA, USA), we assembled a concatenated quality report of the WES data ([Supplementary Table S2](#), available in [www.besjournal.com](http://www.besjournal.com)). The control samples had at least 57 Mb of target exons covered with an average depth of 160.76x (ranging from 112.96x to 243.10x), and the tumor samples had at least 155 Mb of target exons covered with an average depth of 400.22x (ranging from 289.22x to 516.15x). More than 93.03% of tumor-targeted regions were effectively covered by at least 30x reads. [Figure 1](#) shows the schematic of the research process.

Multiple tools were used to identify somatic mutations (SNVs and InDels) in CSCCs. A total of 6,232 mutations involving 3,216 genes in exons and splice regions were detected, including 3,523 missense, 1,561 synonymous, 269 nonsense, 147 splicing, 46 in-frame InDels, 102 frameshift InDels,

448 UTR mutations, 120 5'Flank mutations, and 16 other types of mutations (Supplementary Tables S3–S4, available in www.besjournal.com). Missense mutations were the most frequent type of somatic mutation in the CDS (coding sequence) regions, accounting for 56.53% of all mutations (Figure 2). Each sample had an average of 345 mutations (range, 152–1,030), indicating high heterogeneity among CSCC samples. Lastly, we calculated the aggregated mutation density from non-silent mutations in the CSCC data, resulting in mean and median mutation densities of 2.73/Mb and 1.97/Mb, respectively.

**CNA Analysis** Huang J.<sup>[16]</sup> et al. compared whole-genome sequencing to WES data for somatic CNA analysis in CC, which demonstrated that WES data is also suitable for CNA analysis. In this study, we used WES data to analyze CNAs in CSCCs and identified 6766 CNAs in 30 samples, with an average of 225.87

CNAs per sample. Significant gains or losses of copy number were detected on many chromosome arms in the CSCC samples. Chromosomes 1p, 1q, 3p, 3q, 5p, 16q, 18p, 19q, 20p, and 20q showed frequent copy number gains, whereas chromosomes 4p, 4q, 11p, 11q, 13p, 15q, and 22p showed frequent copy number losses (Supplementary Table S5, available in www.besjournal.com). The overall CNA results were generally consistent with those of other studies on CC<sup>[31-34]</sup>.

Significantly amplified and deleted regions were identified using the GISTIC2.0 algorithm (with a threshold of FDR < 0.20). We subsequently identified 64 focal events, of which 19 were amplification peaks and 45 were deletion peaks. The analysis revealed that these focal events involved 535 genes, some of which are known oncogenes or tumor suppressor genes, such as *FLG* (1q21.3), *BIRC3* (11q22.3), *IRF4* (6p25.3), *TTF1* (9q34.13), *CAMTA1*

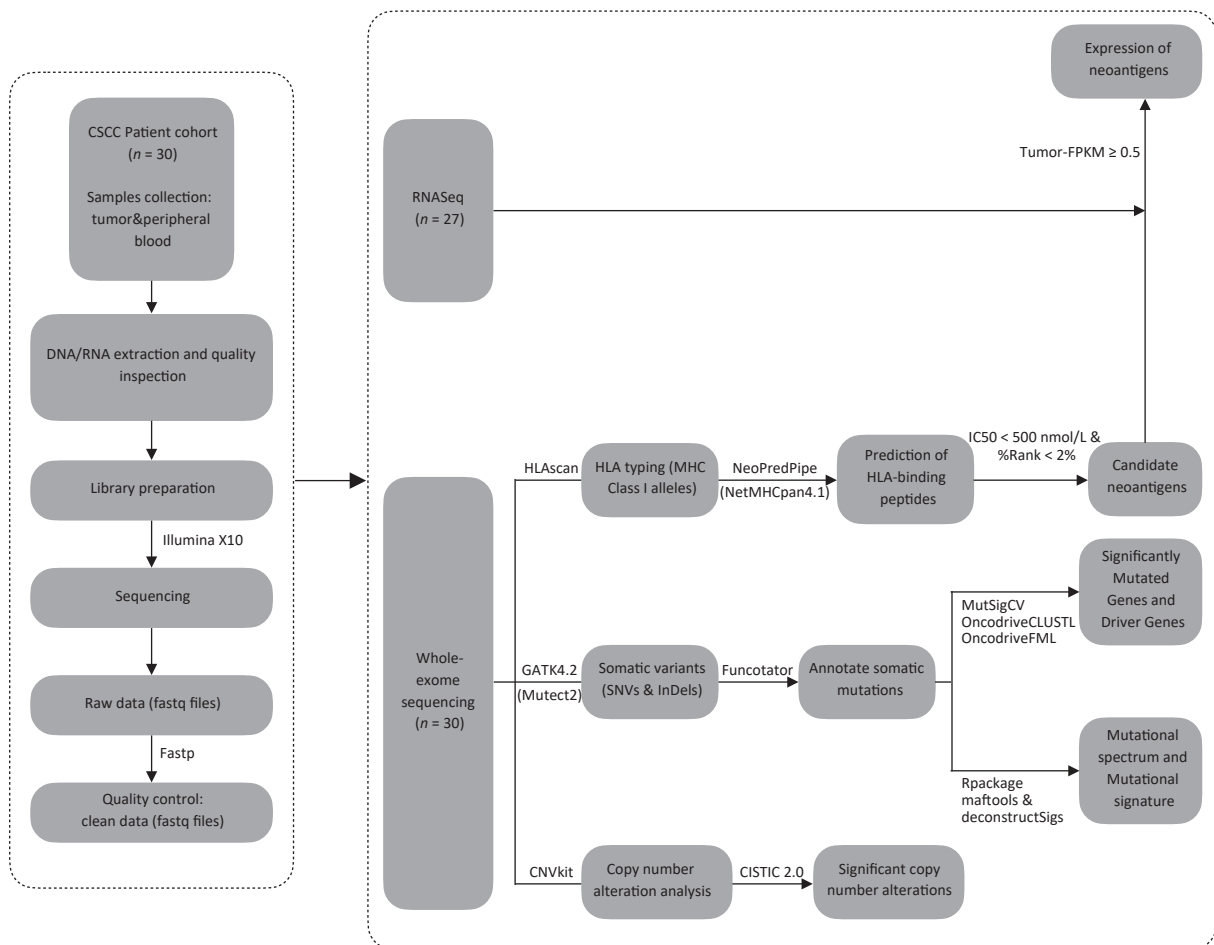


**Figure 1.** The flowchart. CSCC, cervical squamous cell carcinoma. FPKM, Fragments Per Kilobase per Million. HLA, human leukocyte antigen. IC50, half-maximal inhibitory concentration. SNVs, single-nucleotide variants. InDels, insertions and deletions.

(1p36.23), *MUC16* (19p13.2), *ROBO2* (3p12.3), *TAF15* (17q12), and *YWHAE* (17p13.3) (Supplementary Table S6, available in [www.besjournal.com](http://www.besjournal.com)). Among the 64 focal events, significantly amplified cytobands were 3q27.1, 1q21.3, 5p13.2, 7p22.1, and 11q22.3, and significantly deleted regions were 4q13.2, 2q11.2, 7p11.2, 1q21.1, and 11p14.3 (both with the top five lowest *q* values) (Figure 3). The regions with the highest significance in terms of recurrent copy number amplification and deletion were 3q27.1 and 4q13.2, encompassing multiple genes such as *AP2M1*, *DVL3*, *PSMD2*, *EIF2B5*, *ECE2*, *ALG3*, *ABCF3*, *VWA5B2*, *CAMK2N2*, *HTR3C*, *HTR3E*, *MIR1224*, *HTR3E-AS1*, *UGT2B11*, *UGT2B28*, and *LOC105377267*. This result indicated that genes in these two regions may be related to CSCC occurrence.

#### Mutational Spectrum and Mutational Signature

The mutation spectrum displayed the type and number of point mutations in each tumor sample (Figure 4A, B). C>T/G>A transitions (58.38%) and C>G/G>C transversions (23.39%) were the most common point mutations in the present cohort.

Previous studies reported a high C>T transition rate (54%, 55.0%, 63.47%) and a high C>G transversion rate (-, 18.9%, 21.85%) in CC samples through mutation spectrum analysis<sup>[6,16,35]</sup>, which is consistent with the present results. The mutational processes leading to tumorigenesis are diverse, and certain mutational signatures can reveal the specificity of the mutational process and the potential etiology of a cancer<sup>[36]</sup>. To explore this further, we added one base each upstream and downstream from the point mutation site to form a three-base pattern and then counted 96 (6×4×4) mutation combinations. We mapped 96 mutation spectra to the 30 mutational signatures of the COSMIC database<sup>[37]</sup> and identified three mutational signatures in CSCC samples, namely, signature 2 (26.33%), 6 (6.06%) and signature 7 (9.58%) (Figure 4C).

#### SMGs and Driver Genes

The MutSigCV algorithm was applied to identify SMGs across all tumor samples (FDR < 0.20). Then, the top 50 mutated genes of all tumor samples were selected for visualization. In addition to SMGs, the

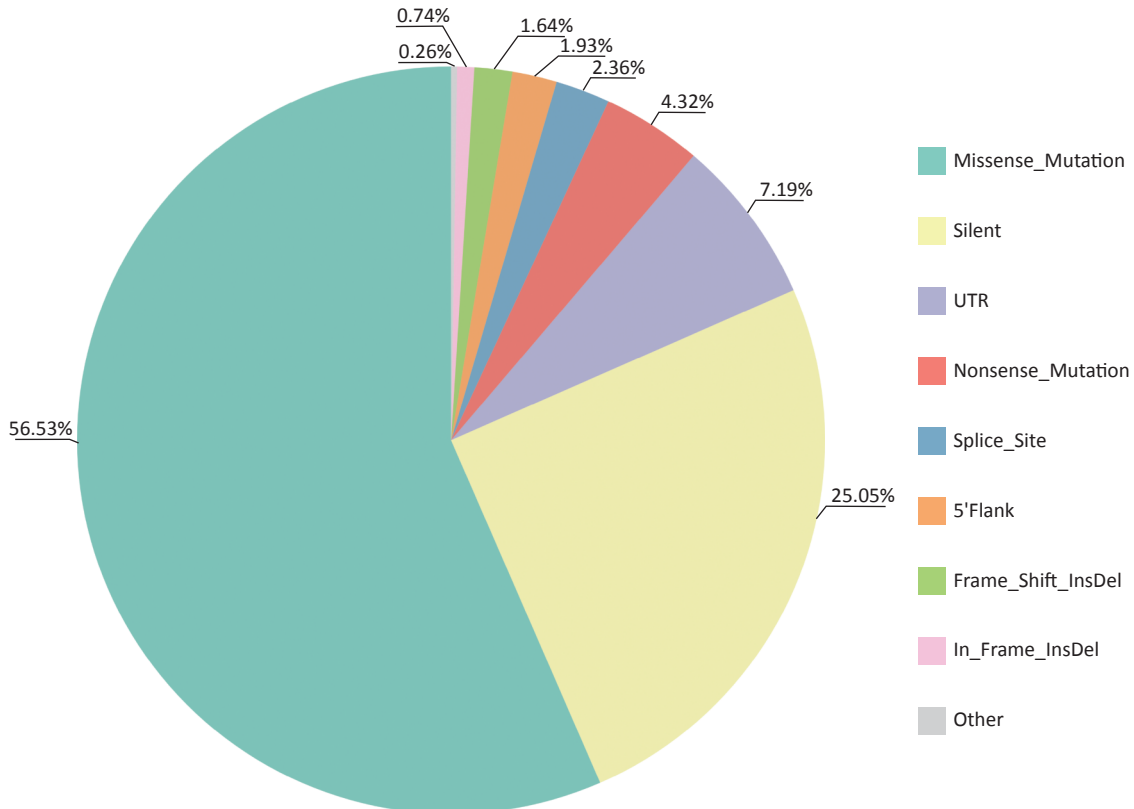


**Figure 2.** Distribution of somatic mutations identified in CSCCs by WES. CSCC, cervical squamous cell carcinoma; WES, whole-exome sequencing.

clinical features of 30 patients, including HPV status, pathology, FIGO stage, and tumor mutation burden (TMB) were determined (Figure 5). Among these genes, *RAMP2* (13.33%, 4/30) and *FOSL2* (13.33%, 4/30) showed statistically significant levels of recurrent mutations (FDR < 0.20) (Supplementary Table S7, available in [www.besjournal.com](http://www.besjournal.com)). They were identified as SMGs in this cohort and confirmed as novel SMGs. Additionally, *PIK3CA* (26.67%, 8/30), *FBXW7* (16.67%, 5/30), *SCN5A* (16.67%, 5/30), *STK11* (16.67%, 5/30), and *PCNXL2* (16.67%, 5/30) had high mutation rates but did not have statistically significant recurrent mutations. However, they were enriched in non-silent mutations, indicating that they may play important roles in C5CC. We identified three driver genes according to the filtering criteria (Table 1). Among the predicted driver genes, *PIK3CA* and *FBXW7* were reported in previous studies<sup>[6,16]</sup>,

and *BICRA* (10.00%, 3/30) is novel. The point mutations of *PIK3CA* were all clustered in the helical domain, including E545K (62.50%, 5/8) and E542K (37.50%, 3/8), whereas no mutations were detected in the kinase domain of the gene (Supplementary Figure S1A, available in [www.besjournal.com](http://www.besjournal.com)). Five hotspot mutations were identified in *FBXW7*, including two R385C (40.00%), one R399G (20.00%), one R425S (20.00%) within the WD40 domain, and one L154fs (20.00%) outside the domain (Supplementary Figure S1B). This mutational characteristic of *FBXW7* has not been reported in previous studies on C5CC.

### Identification of the Neoantigens

In this study, WES data for C5CCs was used to predict neoantigens and RNA-seq data was used to examine the expression of these neoantigens. The

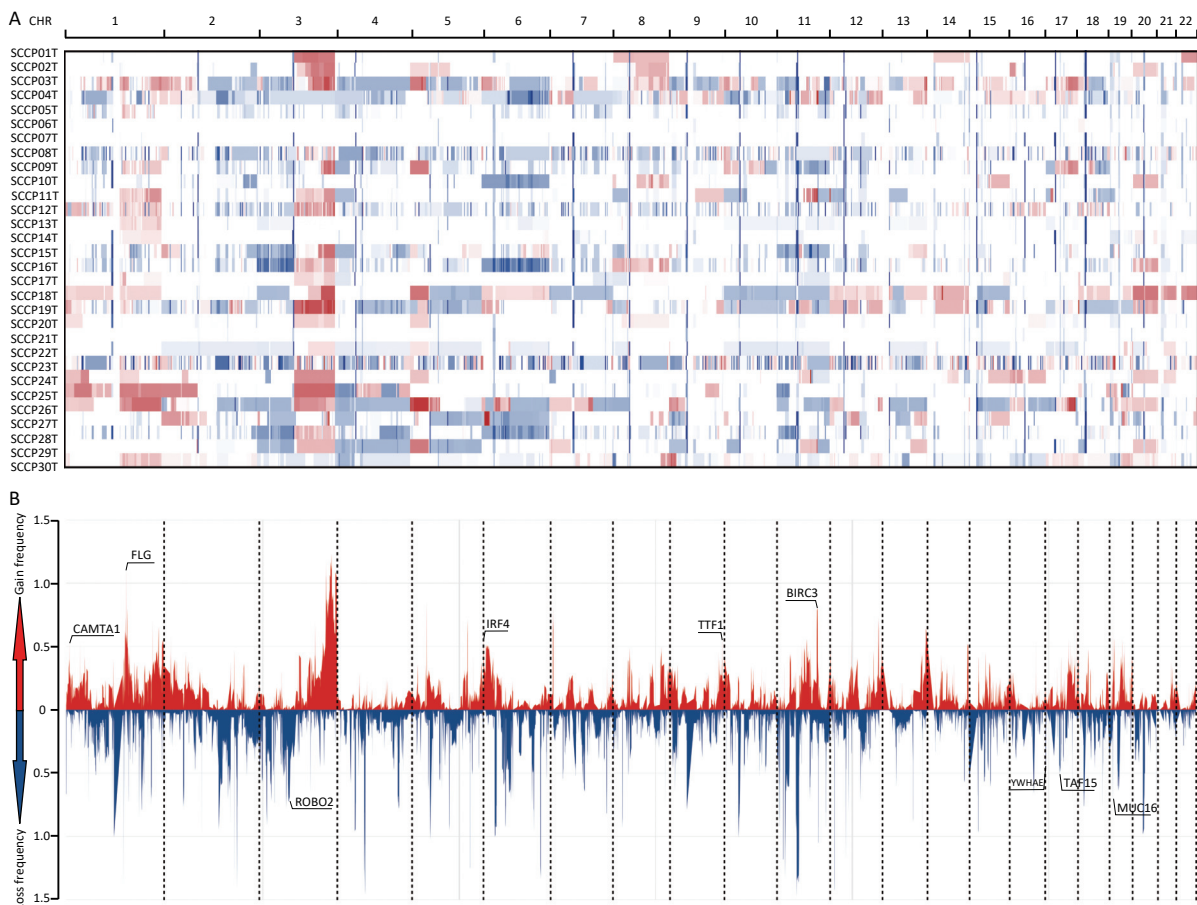


**Figure 3.** Distribution of copy number variations in cervical squamous cell carcinoma. (A) Clustered heatmap of samples. In the heatmap, blue represents downregulated expression, red represents upregulated expression, and white represents no change in expression. (B) Distribution of CNA in the chromosomes. The y-axis shows the variation scores of GISTIC software; the higher the score is, the higher the significance is. CNA, copy number alterations.

HLAscan tool was used to identify four-digit HLA class I alleles in CSCC samples, which showed that HLA-A\*02:01 (33.33%), HLA-B\*13:02 (16.67%), and HLA-C\*06:02 (30.00%) were the most common alleles at the HLA-A, HLA-B, and HLA-C loci respectively (Table 2).

The NeoPredPipe pipeline incorporating the NetMHCpan 4.1 program was applied to predict neoantigens with filtering criteria of IC50 < 500 nmol/L and %Rank < 2%. Potential neoantigens were detectable in all samples, and 4960 potential neoantigens were identified (Supplementary Table S8, available in www.besjournal.com). The average number of non-synonymous mutations in CSCC samples was 136.37 (range, 50–378), with an average of 165.33 neoantigens (range, 44–487) (Table 2). Figure 6 displays the predicted HLA class I neoantigens for each CSCC sample. Pearson correlation analysis showed a strong linear positive correlation between the number of neoantigens and the number of somatic non-synonymous mutations (Pearson correlation coefficient  $R = 0.85$ ,  $P = 3.7 \times 10^{-9}$ ) (Figure 7A), consistent with previous studies<sup>[35,38]</sup>.

The study also identified multiple recurrently

mutated antigen genes, which were defined as “potential neoantigen genes”. Figure 7B shows the potential neoantigen genes at different FIGO stages:

*HDAC6* (3/30), *DPP10* (3/30), *PIK3CA* (8/30), *MUC16* (5/30), *CIC* (3/30), *USP28* (3/30), *DNAH6* (3/30), and *CDKL5* (3/30) (all genes were found in at least three CSCC samples). Most potential neoantigen genes were present in known oncogenic driver genes such as *MUC16*, which promotes cervical cancer progression via JAK2/STAT3 phosphorylation-mediated cyclooxygenase-2 expression<sup>[39]</sup>. Furthermore, *PIK3CA* is an immune-related gene deposited in the Immunology Database and Analysis Portal (ImmPort)<sup>[40]</sup>.

In the present analysis of neoantigens, each unique immune target was detected in a particular CSCC patient, suggesting that neoantigens are highly heterogeneous. This result is consistent with previous reports that the vast majority of potential neoantigens are patient-specific<sup>[41]</sup>. Therefore, we explored the heterogeneity of potential neoantigens in CSCC. The results showed that 99.78% (4949/4960) of the neoantigens were present in only one patient, whereas only 0.22% (11/4,960) of the neoantigens were present in at

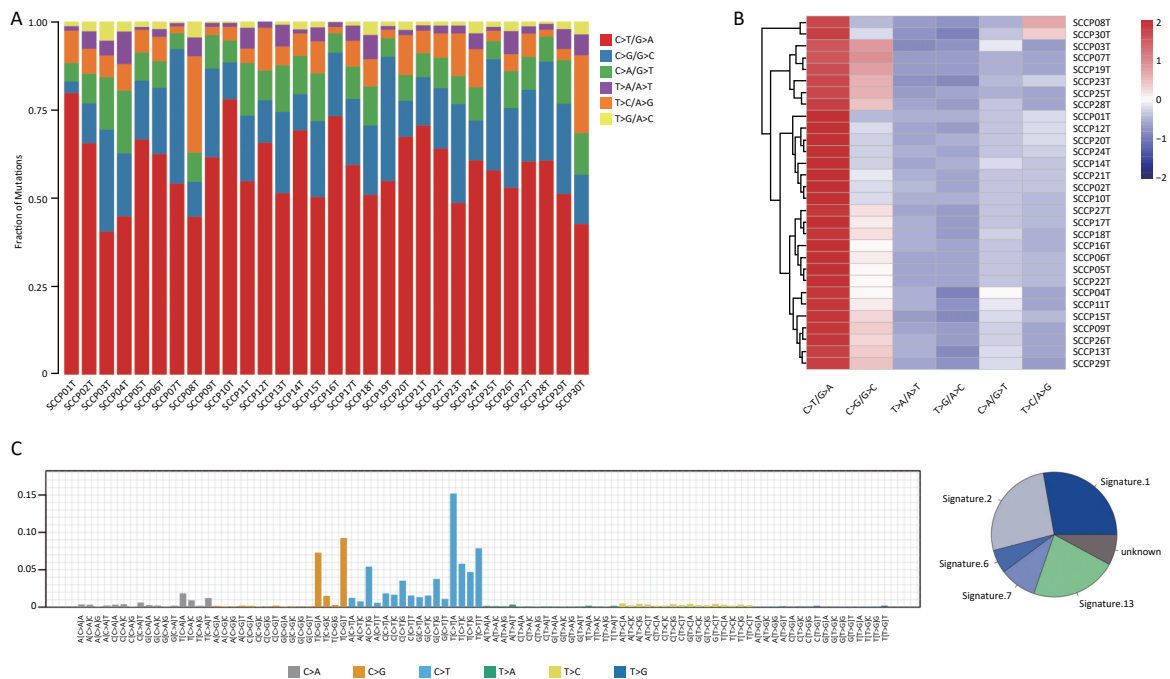


**Figure 4.** Distribution of single-nucleotide variations in different cervical squamous cell carcinoma samples. (A) Column diagram of various mutations identified by WES. (B) Clustered heatmap of various types mutations in 30 cases by WES. (C) Mutational signatures in this study. Proportion of mutational signatures distribution in each group (on the left). Inset pie chart shows the proportion of mutational signatures in each group (on the right). WES, whole-exome sequencing.

least two patients (Figure 7C). “STRDPLSEITK”, generated by *PIK3CA* (E545K), was the most commonly shared neoantigen. This result suggests that identifying shared neoantigens for CSCC could be challenging.

RNA-seq data were used to examine the expression of neoantigens, and the results showed that there were 4,559 potential neoantigens in 27 pairs of samples, of which 58.13% (2,650/4,559, 2,650 neoantigens involving 939 genes) were expressed (Supplementary Table S9, available in www.besjournal.com).

**Validation of Potential Neoantigens**

The Tumor-Specific Neoantigen database (TSNadb) is a collection of neoantigen information from 7748 samples of 16 different cancers in TCGA database<sup>[42]</sup>. CTdatabase contains high-throughput and carefully curated data on cancer-testis antigens<sup>[43]</sup>. The accuracy of the present neoantigen results was verified by comparison with TCGA-CESC (cervical squamous cell carcinoma and endocervical adenocarcinoma) data in TSNadb and CTA data in CTdatabase. Among the 4,960 potential

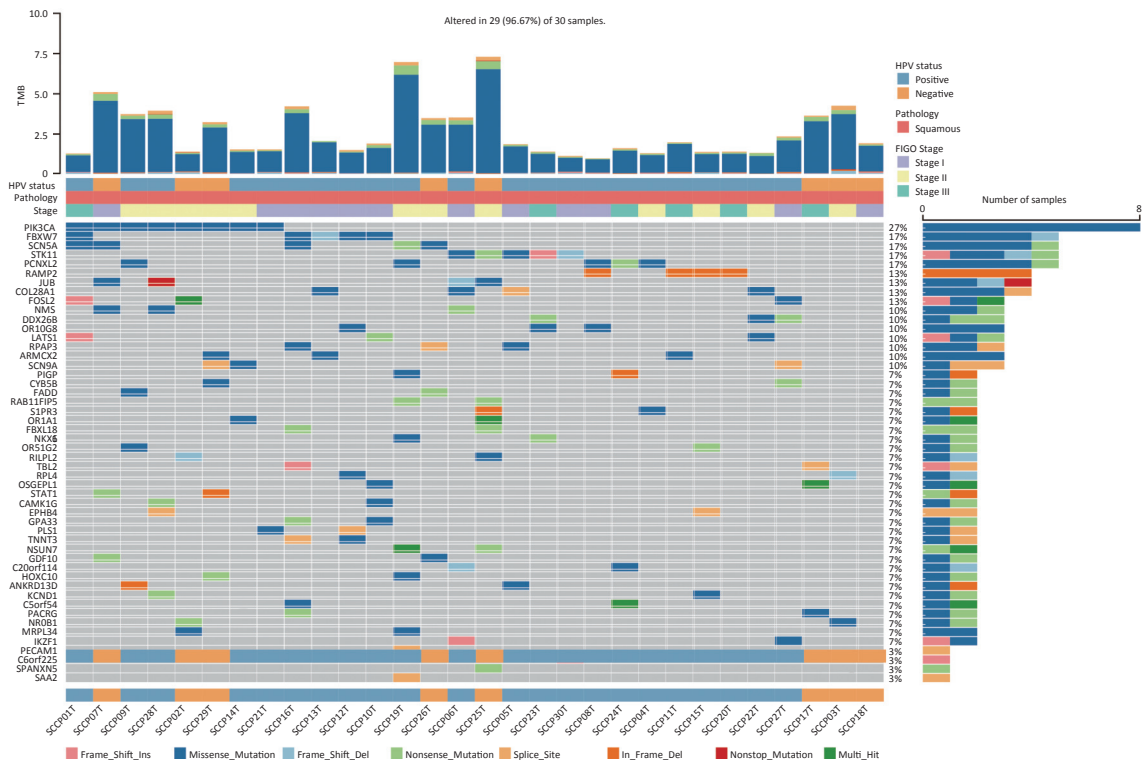


**Figure 5.** The alteration spectrum of the top 50 significantly mutated genes in 30 cervical squamous cell carcinoma samples. TMB, tumor mutation burden. HPV, human papillomavirus. FIGO, International Federation of Gynecology and Obstetrics.

**Table 1.** Driver genes identified by whole exome sequencing

Gene	Indels	SNVs	Tot Muts	Sample affect	Sample percent (%)	FDR CT <sup>‡</sup>			Present in CGC	Reported in previous research
						Predicted by OncodriveCLUSTL	Predicted by OncodriveFML	Predicted by MutSigCV		
<i>K3CAPI</i>	0	8	8	8	26.67	0.048	0.181	0.836	Yes	Yes
<i>BICRA</i>	0	3	3	3	10.00	0.181	0.064	1	No	No
<i>FBXW7</i>	1	4	5	5	16.67	0.181	0.165	1	Yes	Yes

**Note.** <sup>\*</sup>Tot Muts denotes the total mutations occurred in certain genes. <sup>‡</sup>FDR CT denotes corrected *P* value. FDR, false discovery rate; SNVs, single-nucleotide variants; InDels, insertions and deletions; CGC, Cancer Gene Census.

neoantigens identified in this study, 114 neoantigens involving 27 genes were identified in both databases. In TSNAdb, 46 neoantigens corresponding to eight genes were identified in TCGA-CESC dataset (Table 3), whereas in CTdatabase (CTAs), 68 neoantigens corresponding to 19 genes were identified (Supplementary Table S10, available in www.besjournal.com). Six of the 27 neoantigen-related genes were reported as therapeutic targets in the Therapeutic Target

Database<sup>[44]</sup> and the corresponding drugs were also included. Alpelisib and BAY 80-6956, which are related to the *PIK3CA* target, have been approved by the FDA for the treatment of breast cancer and follicular lymphoma, respectively<sup>[45,46]</sup>, whereas drugs targeting *MAPK1*, *MUC16*, *MAGEA3*, *MAGEC2*, and *MAGEC1* are currently in clinical trials. Additionally, *PIK3CA* was included in a clinical trial as a potential therapeutic target in the treatment of CC (NCT02957266).

**Table 2.** Number of nonsynonymous mutations, neoantigens and HLA class I allotypes of 30 patients

Sample-ID	Number of nonsynonymous mutations	Number of neoantigens	HLA-A*	HLA-B*	HLA-C*	Sequencing strategies	Stage
SCCP01T	66	52	02:07/30:01	—	01:02/12:02	WES/RNA-seq	IIIC1
SCCP02T	72	86	24:02/33:03	58:01	01:02/03:02	WES	IIA2
SCCP03T	220	258	02:01/03:01	35:08/44:02	05:03	WES/RNA-seq	IIA
SCCP04T	67	97	03:01/31:01	51:02	12:02/15:02	WES/RNA-seq	IIB
SCCP05T	96	119	02:01/11:01	51:01/51:02	08:01/15:02	WES/RNA-seq	IB2
SCCP06T	182	311	02:01/02:06	51:01	03:03/15:02	WES/RNA-seq	IB2
SCCP07T	264	163	03:01	35:01	04:01	WES/RNA-seq	IB3
SCCP08T	50	76	11:01/30:01	13:02	03:04/06:02	WES/RNA-seq	IB2
SCCP09T	193	333	11:01/24:02	13:01/15:01	03:03/03:04	WES/RNA-seq	IIA
SCCP10T	98	151	02:01/02:03	13:01/48:01	03:04/08:03	WES/RNA-seq	IB2
SCCP11T	102	115	02:07/31:01	40:01	01:02/03:04	WES/RNA-seq	IIIA
SCCP12T	77	124	02:01/30:01	15:02/44:03	08:01	WES/RNA-seq	IB1
SCCP13T	106	128	02:01/02:07	40:01/54:01	01:02/03:04	WES/RNA-seq	IB3
SCCP14T	79	109	02:06/11:01	40:01/40:06	01:02/08:01	WES/RNA-seq	IIA1
SCCP15T	71	51	01:01/11:01	37:01	06:02/07:02	WES/RNA-seq	IIA1
SCCP16T	218	290	02:01/02:06	15:11/35:01	03:03	WES	IB2
SCCP17T	188	271	02:06/24:02	15:11/51:01	03:03/14:02	WES/RNA-seq	IIIC1
SCCP18T	99	128	02:03/03:01	27:07/40:01	07:02/15:02	WES/RNA-seq	IB3
SCCP19T	361	487	01:01/02:06	07:02/51:01	07:02/14:02	WES/RNA-seq	IIA1
SCCP20T	72	67	03:01	07:02/37:01	06:02/07:02	WES/RNA-seq	IIIC1
SCCP21T	79	121	11:01/24:02	15:02/27:07	08:01/15:02	WES/RNA-seq	IB2
SCCP22T	68	53	02:01/03:01	13:02/	03:03/06:02	WES/RNA-seq	IIB
SCCP23T	72	90	01:01/11:01	35:03/37:01	06:02/12:03	WES/RNA-seq	IIIC1
SCCP24T	83	66	02:01	15:11	03:03/08:01	WES/RNA-seq	IIIC1
SCCP25T	378	324	01:01/30:01	13:02/54:01	01:02/06:02	WES/RNA-seq	IIA1
SCCP26T	180	118	02:07/33:03	37:01/46:01	01:02/06:02	WES/RNA-seq	IIA1
SCCP27T	121	186	11:01/30:01	13:02/14:01	06:02/08:02	WES/RNA-seq	IB2
SCCP28T	204	392	11:01/11:12	15:02/35:03	08:01/12:03	WES/RNA-seq	IIA2
SCCP29T	167	150	11:01	13:01/13:02	03:04/06:02	WES/RNA-seq	IIA
SCCP30T	58	44	02:01/32:01	13:01	03:04/12:02	WES	IB1

**Note.** HLA, human leukocyte antigen. \*List separator.

**DISCUSSION**

There is limited data on genomic alteration profiles and neoantigens of CSCC in Chinese patients. In this study, we used WES to analyze the somatic mutational landscape in a cohort of patients with

CSCC (30 samples). Analysis of somatic non-synonymous mutations was used to identify potential neoantigens that can serve as new targets for CSCC immunotherapy. RNA-seq data was used to examine the expression of candidate neoantigens.

A total of 6,232 somatic mutations were

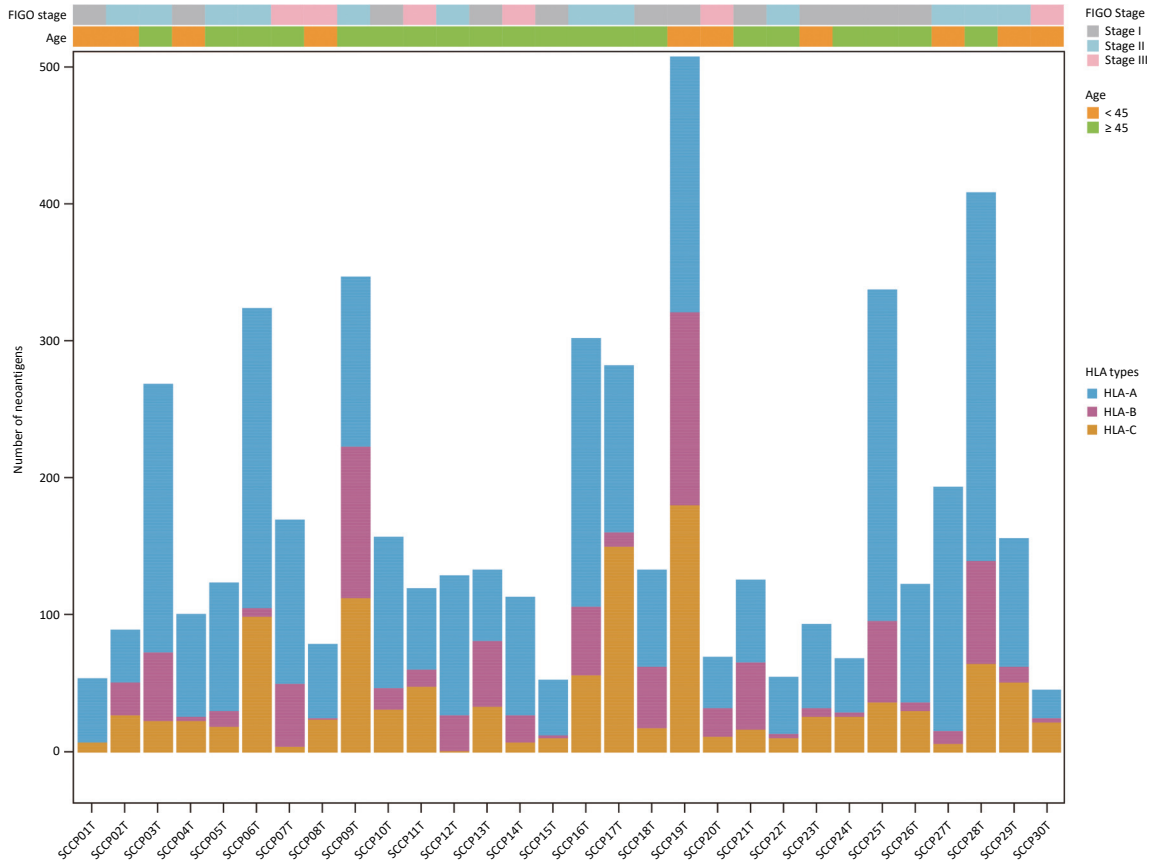


**Figure 6.** Predicted HLA class I neoantigens in 30 squamous cell carcinoma. Different colors represented different HLA types. HLA, human leukocyte antigen.

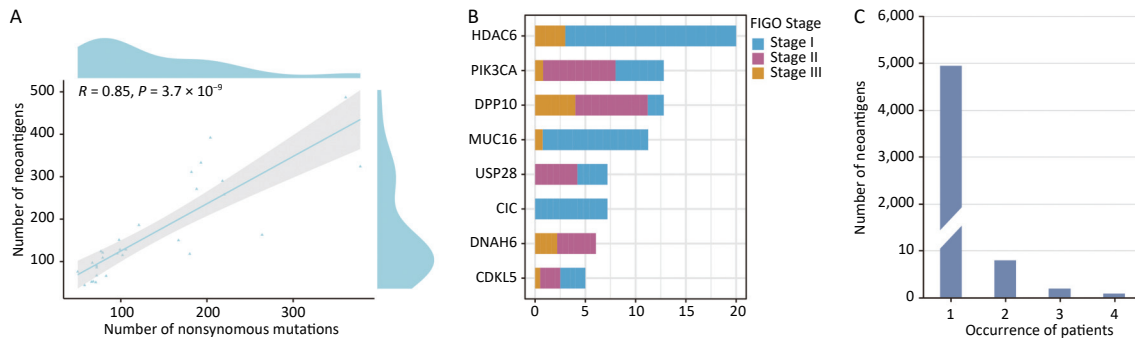


**Figure 7.** Distribution of potential neopeptides genes in different stages of CSCC. (A) Correlation between the number of mutations and the number of exome-derived neopeptides (Pearson’s correlation coefficient,  $R = 0.85$ ,  $P < 0.001$ ). (B) Barplots showed the number of potential neoantigen genes in CSCCs. (C) Neoantigen recurrence in our cohort. CSCC, cervical squamous cell carcinoma. FIGO, International Federation of Gynecology and Obstetrics.

**Table 3.** A list of candidate neoantigens validated by TSNAdb database

Sample	Protein	Mutation AA	HLA types	Identity	Length (AA)	%Rank	Affinity (nmol/L)	Drugs
SCCP14T	CADPS	R737W	HLA-A02:06	YLRDLLEWA	9	0.502	25.53	-
SCCP14T	CADPS	R737W	HLA-B40:01	LEWAENGAM	9	0.436	52.67	-
SCCP14T	CADPS	R737W	HLA-B40:01	LEWAENGAMI	10	1.173	237.85	-
SCCP24T	CADPS	R737W	HLA-A02:01	YLRDLLEWA	9	0.407	24.09	-
SCCP13T	DENND5B	D339H	HLA-A02:01	FLHAPVPYL	9	0.007	3.86	-
SCCP13T	DENND5B	D339H	HLA-A02:01	SLLHFLHAPV	10	0.526	5.35	-
SCCP13T	DENND5B	D339H	HLA-A02:01	FLHAPVPYLM	10	0.469	13.82	-
SCCP13T	DENND5B	D339H	HLA-C03:04	FLHAPVPYL	9	0.133	34.66	-
SCCP13T	DENND5B	D339H	HLA-A02:01	HFLHAPVPYL	10	1.087	44.79	-
SCCP13T	DENND5B	D339H	HLA-B54:01	LPASLLHFLHA	11	0.194	52.16	-
SCCP13T	DENND5B	D339H	HLA-A02:07	FLHAPVPYL	9	0.014	256.91	-
SCCP13T	DENND5B	D339H	HLA-A02:01	LHFLHAPVPYL	11	1.597	272.86	-
SCCP13T	DENND5B	D339H	HLA-C01:02	HAPVPYLMGL	10	0.187	380.05	-
SCCP13T	DENND5B	D339H	HLA-C01:02	FLHAPVPYL	9	0.129	391.67	-
SCCP13T	DENND5B	D339H	HLA-A02:01	SLLHFLHAP	9	1.536	453.38	-
SCCP07T	MAPK1	E322K	HLA-C04:01	YYDPSDKPI	9	0.017	389.35	BVD-523, ASTX029, HH2710
SCCP01T	MAPK1	R135K	HLA-A30:01	KGLKYIHSA	9	1.615	482.21	BVD-523, ASTX029, HH2711
SCCP06T	MUC16	A4577T	HLA-A02:01	SMGDTLASI	9	0.265	30.46	Oregovomab, Abagovomab
SCCP06T	MUC16	A4577T	HLA-A02:06	SMGDTLASI	9	0.523	58.48	Oregovomab, Abagovomab
SCCP06T	MUC16	A4577T	HLA-A02:01	SMGDTLASISI	11	1.565	324.65	Oregovomab, Abagovomab
SCCP06T	MUC16	A4577T	HLA-C15:02	SSMGDTLASI	10	1.661	353.86	Oregovomab, Abagovomab
SCCP07T	PIK3CA	E542K	HLA-A03:01	AISTRDPLSK	10	0.14	53.93	Alpelisib, BAY 80-6946
SCCP07T	PIK3CA	E542K	HLA-A03:01	KAISTRDPLSK	11	0.299	469.89	Alpelisib, BAY 80-6947
SCCP09T	PIK3CA	E542K	HLA-A11:01	AISTRDPLSK	10	0.312	99.32	Alpelisib, BAY 80-6948
SCCP09T	PIK3CA	E542K	HLA-A11:01	KAISTRDPLSK	11	0.273	256.36	Alpelisib, BAY 80-6949
SCCP09T	PIK3CA	E542K	HLA-A11:01	ISTRDPLSK	9	0.629	333.21	Alpelisib, BAY 80-6950
SCCP21T	PIK3CA	E542K	HLA-A11:01	AISTRDPLSK	10	0.312	99.32	Alpelisib, BAY 80-6951
SCCP21T	PIK3CA	E542K	HLA-A11:01	KAISTRDPLSK	11	0.273	256.36	Alpelisib, BAY 80-6952
SCCP21T	PIK3CA	E542K	HLA-A11:01	ISTRDPLSK	9	0.629	333.21	Alpelisib, BAY 80-6953
SCCP21T	PIK3CA	E542K	HLA-C15:02	STRDPLSKI	9	0.135	453.03	Alpelisib, BAY 80-6954
SCCP01T	PIK3CA	E545K	HLA-A30:01	STRDPLSEITK	11	0.01	38.96	Alpelisib, BAY 80-6955
SCCP02T	PIK3CA	E545K	HLA-B58:01	ITKQEKDFLW	10	0.049	13.03	Alpelisib, BAY 80-6956
SCCP02T	PIK3CA	E545K	HLA-B58:01	EITKQEKDFLW	11	1.03	391.32	Alpelisib, BAY 80-6957
SCCP14T	PIK3CA	E545K	HLA-A11:01	STRDPLSEITK	11	0.053	91.72	Alpelisib, BAY 80-6958
SCCP28T	PIK3CA	E545K	HLA-A11:12	STRDPLSEITK	11	0.053	91.72	Alpelisib, BAY 80-6959
SCCP28T	PIK3CA	E545K	HLA-A11:01	STRDPLSEITK	11	0.053	91.72	Alpelisib, BAY 80-6960
SCCP29T	PIK3CA	E545K	HLA-A11:01	STRDPLSEITK	11	0.053	91.72	Alpelisib, BAY 80-6961
SCCP03T	SLC26A3	V340I	HLA-C05:03	VGDCFDIAM	9	0.841	391.96	-
SCCP19T	VCPIP1	D434N	HLA-A02:06	GIHPSLVANV	10	0.749	171.9	-
SCCP19T	VCPIP1	D434N	HLA-A01:01	VANVHQYFY	9	0.173	244.29	-

Continued

Sample	Protein	Mutation AA	HLA types	Identity	Length (AA)	%Rank	Affinity (nmol/L)	Drugs
SCCP19T	VCPIP1	D434N	HLA-C14:02	LVANVHQYF	9	1.247	361.85	-
SCCP19T	VCPIP1	D434N	HLA-A01:01	LVANVHQYFY	10	0.643	448.15	-
SCCP28T	ZBED4	E664K	HLA-B15:02	KMIALDLQPY	10	1.429	89.83	-
SCCP28T	ZBED4	E664K	HLA-C12:03	IAKMIALDL	9	0.66	132.87	-
SCCP28T	ZBED4	E664K	HLA-A11:12	VAKKITSLIAK	11	1.798	386.39	-
SCCP28T	ZBED4	E664K	HLA-A11:01	VAKKITSLIAK	11	1.798	386.39	-

**Note.** AA, amino acids. HLA, human leukocyte antigen.

identified in 30 CSCC samples, with an average of 207.73 mutations per sample, which is slightly lower than the average of 225.65 mutations per sample in TCGA database for CC<sup>[6]</sup>. Analysis of nonsilent mutations showed a mean mutation burden of 2.73/Mb, which was slightly higher than TCGA mutational burden of 2.53/Mb (excluding hypermutated tumors)<sup>[6]</sup>. Chung<sup>[34]</sup> et al. reported that cervical adenocarcinoma has a lower mutational burden than CSCC, which may explain the difference in mutational burden between this study and TCGA database. CNA analysis in CSCC identified 6,766 CNAs (225.87 per sample), which is considerably higher than the number reported in TCGA database for CC<sup>[6]</sup>. GISTIC2.0 analysis revealed 19 amplification peaks and 45 deletion peaks. Furthermore, 15 (50%) patients had high-level copy number amplification at 3q27.1, which was consistent with findings in lung squamous cell carcinoma and esophageal squamous cell carcinoma<sup>[47,48]</sup>. *ALG3*, which is one of the genes covered by this region, helps tumor cells generate high mannose N-linked glycans. Aberrant expression of high-mannose N-linked glycans is associated with cancer progression<sup>[49,50,51]</sup>. *ALG3* is significantly overexpressed in radioresistant breast cancer tissues and promotes radioresistance and cancer stemness by inducing the glycosylation of TGF- $\beta$  receptor II (TGFBR2)<sup>[50]</sup>. Although *ALG3* is an effective therapeutic target in breast cancer patients with high *ALG3* levels<sup>[50]</sup>, whether it promotes the development of CSCC remains to be determined. *HTR3C*, another gene in the 3q27.1 region, is a biomarker for predicting lung cancer prognosis<sup>[52]</sup>. A risk model that includes *HTR3E* together with 13 other central immune-related genes (*CBLC*, *TNF*, *PSMC4*, *TRAV30*, *PDIA3*, *FGF8*, *PDGFRA*, *ESRRA*, *SBDS*, *CRHR1*, *LTA*, *NR2F1*, *TNFRSF18*) was used to predict the prognosis of endometrial carcinoma<sup>[53]</sup>. *MIR1224* acts as a tumor suppressor in the occurrence and development of cancers and can be used as a tumor biomarker for early diagnosis and

prognosis prediction<sup>[54]</sup>. *UGT2B28* (located at 4q13.2) is a predictor of progression in prostate cancer and can be therapeutically targeted by using a combination of AR/EGFR inhibitors<sup>[55]</sup>.

Analysis of CSCC samples identified three mutational signatures corresponding to signatures 2, 6, and 7 in the COSMIC database (Figure 4C). These are slightly different from those found in the CESC dataset in TCGA database, specifically signature 2 (72.5%) and 6 (13.2%). The APOBEC family of proteins specifically catalyze the conversion of cytosine in the genome to uracil, which is related to base excision repair and DNA replication mechanisms<sup>[56]</sup>. It can be activated by HPV virus infection and is involved in the immune response<sup>[56]</sup>. APOBEC, which is closely related to cervical carcinogenesis, is the source of signature 2 and signature 13 in human cancers<sup>[6,57]</sup>. These studies suggest that APOBEC causes CSCC mutations under the control of HPV. Additionally, signature 6 is a novel early warning biomarker for CC associated with the deficiency of DNA mismatch repair.

This study identified three genes (*PIK3CA*, *FBXW7*, and *BICRA*) predicted to act as driver genes that could potentially promote tumor formation and development. *BICRA*, a component of the SWI/SNF chromatin remodeling complex, was identified as a novel driver gene of CSCC. However, we did not find published evidence supporting that this gene is associated with cancer risk or development. We observed eight missense mutations in *PIK3CA* (26.67%), which is consistent with results reported previously (26% in Cancer Genome Atlas Research Network<sup>[6]</sup>, 16.7% in Huang et al.<sup>[16]</sup>). The results further indicated no significant difference in the *PIK3CA* mutation rate between cervical adenocarcinoma and CSCC. We identified two SMGs that may be associated with CSCC: *RAMP2* and *FOSL2*. *RAMP2* downregulation may promote distant metastasis of cancers and is associated with a low survival rate in oral squamous cell carcinoma<sup>[58,59]</sup>,

whereas *FOSL2* is closely related to the occurrence of ovarian cancer, lung cancer, and breast cancer<sup>[60,61,62]</sup>. The results indicate that these two genes may play crucial roles in the occurrence and development of tumors. However, further studies are needed to validate these findings and to develop these factors as potential biomarkers for CSCC.

Antigen presentation plays a crucial role in the human immune response to cancer. Immunotherapies for cancer are often based on targeting antigens presented by major histocompatibility complex/HLA molecules<sup>[63]</sup>. Significant advances have been made in immunotherapy strategies for the treatment of solid tumors (such as breast cancer, prostate cancer, and non-small cell lung cancer). However, the currently available approaches are not sufficient to cure CC. Neoantigens are optimal targets for immunotherapy and are up-and-coming therapeutic options. We identified 4960 neoantigens in this study and found that the number of neoantigens was positively correlated with the number of somatic non-synonymous mutations, whereas it showed no obvious correlation with clinical stage. *HDAC6* and *DPP10* are two potential neoantigen genes that are detected in the early stage of CSCC. *HDAC6* is a unique HDAC family member that regulates the Ras/MAPK/ERK, PI3K/Akt, and Wnt signaling pathways, which are associated with cellular proliferation and are activated in most tumors<sup>[64]</sup>. Liu et al. suggested that *DPP10* inhibits colon cancer stem cell proliferation by regulating microRNAs such as miR-127-3p<sup>[65]</sup>. A previous study demonstrated that *DPP10* methylation levels are significantly correlated with cervical neoplasia progression<sup>[66]</sup>. We found that almost every neoantigen was present in one sample, further highlighting the difficulty in ubiquitous neoantigen identification in CSCC. We used RNA-seq data to examine the expression of neoantigens and found that five potential neoantigen genes (including *PIK3CA*, *MUC16*, *USP28*, *CIC*, and *CDKL5*) were expressed. Further extended clinical studies are needed to determine whether these genes are of value for CSCC immunotherapy. The validation with two available neoantigen-related public databases (TSNadb and CTdatabase) identified 114 neoantigens involving 27 genes that may serve as candidate targets for neoantigen vaccines.

## CONCLUSION

In this study, the comprehensive genomic

characteristics of CSCC were determined using WES data. WES and RNA-seq data were used to narrow the scope of neoantigens for individualized immunotherapy in CSCC. Further experimental verification is needed to obtain effective neoantigens.

## AUTHOR CONTRIBUTIONS

Conceptualization: Meng Wu and Yuanguang Meng. Material preparation, data collection and analysis: Meng Wu and Jialu Zhou. Formal analysis: Meng Wu and Zhe Zhang. Writing-original draft: Meng Wu. Writing, review and editing: Meng Wu, Yuanguang Meng, and Zhe Zhang. All authors read and approved the final manuscript.

## DATA AVAILABILITY STATEMENT

The data that support the findings of this study are available on reasonable request from the corresponding author. Requests may be sent to: meng6512@vip.sina.com.

Received: September 15, 2023;

Accepted: February 23, 2024

## REFERENCES

1. Sung H, Ferlay J, Siegel RL, et al. Global cancer statistics 2020: GLOBOCAN estimates of incidence and mortality worldwide for 36 cancers in 185 countries. *CA Cancer J Clin*, 2021; 71, 209–49.
2. Singh D, Vignat J, Lorenzoni V, et al. Global estimates of incidence and mortality of cervical cancer in 2020: a baseline analysis of the WHO global cervical cancer elimination initiative. *Lancet Glob Health*, 2023; 11, e197–206.
3. Xia CF, Dong XS, Li H, et al. Cancer statistics in China and United States, 2022: profiles, trends, and determinants. *Chin Med J (Engl)*, 2022; 135, 584–90.
4. Cohen PA, Jhingran A, Oaknin A, et al. Cervical cancer. *Lancet*, 2019; 393, 169–82.
5. Wu X, Peng L, Zhang YO, et al. Identification of key genes and pathways in cervical cancer by bioinformatics analysis. *Int J Med Sci*, 2019; 16, 800–12.
6. The Cancer Genome Atlas Research Network. Integrated genomic and molecular characterization of cervical cancer. *Nature*, 2017; 543, 378–84.
7. Lei JY, Ploner A, Elfström KM, et al. HPV vaccination and the risk of invasive cervical cancer. *N Engl J Med*, 2020; 383, 1340–8.
8. Jin X, Liu ZR, Yang DX, et al. Recent progress and future perspectives of immunotherapy in advanced gastric cancer. *Front Immunol*, 2022; 13, 948647.
9. Fournel L, Wu ZR, Stadler N, et al. Cisplatin increases PD-L1 expression and optimizes immune check-point blockade in non-small cell lung cancer. *Cancer Lett*, 2019; 464, 5–14.
10. Solis RN, Silverman DA, Birkeland AC. Current trends in

- precision medicine and next-generation sequencing in head and neck cancer. *Curr Treat Options Oncol*, 2022; 23, 254–67.
11. Monk BJ, Enomoto T, Kast WM, et al. Integration of immunotherapy into treatment of cervical cancer: recent data and ongoing trials. *Cancer Treat Rev*, 2022; 106, 102385.
  12. Wang RJ, Pan W, Jin L, et al. Human papillomavirus vaccine against cervical cancer: opportunity and challenge. *Cancer Lett*, 2020; 471, 88–102.
  13. Ferrall L, Lin KY, Roden RBS, et al. Cervical cancer immunotherapy: facts and hopes. *Clin Cancer Res*, 2021; 27, 4953–73.
  14. Peng M, Mo YZ, Wang YA, et al. Neoantigen vaccine: an emerging tumor immunotherapy. *Mol Cancer*, 2019; 18, 128.
  15. Lang F, Schrörs B, Löwer M, et al. Identification of neoantigens for individualized therapeutic cancer vaccines. *Nat Rev Drug Discov*, 2022; 21, 261–82.
  16. Huang J, Qian ZY, Gong YH, et al. Comprehensive genomic variation profiling of cervical intraepithelial neoplasia and cervical cancer identifies potential targets for cervical cancer early warning. *J Med Genet*, 2019; 56, 186–94.
  17. Li H. (2013) Aligning sequence reads, clone sequences and assembly contigs with BWA-MEM. arXiv: 1303.3997v2 [q-bio.GN].
  18. McKenna A, Hanna M, Banks E, et al. The genome analysis toolkit: a MapReduce framework for analyzing next-generation DNA sequencing data. *Genome Res*, 2010; 20, 1297–303.
  19. McKenna A, Hanna M, Banks E, et al. The Genome Analysis Toolkit: a MapReduce framework for analyzing next-generation DNA sequencing data. *Genome Res*, 2010; 20(9), 1297–1303.
  20. Talevich E, Shain AH, Botton T, et al. CNVkit: genome-wide copy number detection and visualization from targeted DNA sequencing. *PLoS Comput Biol*, 2016; 12, e1004873.
  21. Robinson JT, Thorvaldsdóttir H, Wenger AM, et al. Variant review with the integrative genomics viewer. *Cancer Res*, 2017; 77, e31–4.
  22. Mermel CH, Schumacher SE, Hill B, et al. GISTIC2.0 facilitates sensitive and confident localization of the targets of focal somatic copy-number alteration in human cancers. *Genome Biol*, 2011; 12, R41.
  23. Mayakonda A, Lin DC, Assenov Y, et al. Maftools: efficient and comprehensive analysis of somatic variants in cancer. *Genome Res*, 2018; 28, 1747–56.
  24. Rosenthal R, McGranahan N, Herrero J, et al. deconstructSigs: delineating mutational processes in single tumors distinguishes DNA repair deficiencies and patterns of carcinoma evolution. *Genome Biol*, 2016; 17, 31.
  25. Arnedo-Pac C, Mularoni L, Muiños F, et al. OncodriveCLUSTL: a sequence-based clustering method to identify cancer drivers. *Bioinformatics*, 2019; 35, 4788–90.
  26. Mularoni L, Sabarinathan R, Deu-Pons J, et al. OncodriveFML: a general framework to identify coding and non-coding regions with cancer driver mutations. *Genome Biol*, 2016; 17, 128.
  27. Lawrence MS, Stojanov P, Polak P, et al. Mutational heterogeneity in cancer and the search for new cancer-associated genes. *Nature*, 2013; 499, 214–8.
  28. Ka S, Lee S, Hong J, et al. HLAScan: genotyping of the HLA region using next-generation sequencing data. *BMC Bioinformatics*, 2017; 18, 258.
  29. Schenck RO, Lakatos E, Gatenbee C, et al. NeoPredPipe: high-throughput neoantigen prediction and recognition potential pipeline. *BMC Bioinformatics*, 2019; 20, 264.
  30. Reynisson B, Alvarez B, Paul S, et al. NetMHCpan-4.1 and NetMHCIIpan-4.0: improved predictions of MHC antigen presentation by concurrent motif deconvolution and integration of MS MHC eluted ligand data. *Nucleic Acids Res*, 2020; 48, W449–54.
  31. Ojesina AI, Lichtenstein L, Freeman SS, et al. Landscape of genomic alterations in cervical carcinomas. *Nature*, 2014; 506, 371–5.
  32. Niyazi M, Han LL, Husaiyin S, et al. Analysis of somatic mutations and key driving factors of cervical cancer progression. *Open Med (Wars)*, 2023; 18, 20230759.
  33. Xu YX, Luo H, Hu QC, et al. Identification of potential driver genes based on multi-genomic data in cervical cancer. *Front Genet*, 2021; 12, 598304.
  34. Chung TKH, Van Hummelen P, Chan PKS, et al. Genomic aberrations in cervical adenocarcinomas in Hong Kong Chinese women. *Int J Cancer*, 2015; 137, 776–83.
  35. Bao CH, An N, Xie H, et al. Identifying potential neoantigens for cervical cancer immunotherapy using comprehensive genomic variation profiling of cervical intraepithelial neoplasia and cervical cancer. *Front Oncol*, 2021; 11, 672386.
  36. Alexandrov LB, Nik-Zainal S, Wedge DC, et al. Signatures of mutational processes in human cancer. *Nature*, 2013; 500, 415–21.
  37. Tate JG, Bamford S, Jubb HC, et al. COSMIC: the catalogue of somatic mutations in cancer. *Nucleic Acids Res*, 2019; 47, D941–7.
  38. Chen YP, Zhang Y, Lv JW, et al. Genomic analysis of tumor microenvironment immune types across 14 solid cancer types: immunotherapeutic implications. *Theranostics*, 2017; 7, 3585–94.
  39. Shen H, Guo M, Wang L, et al. MUC16 facilitates cervical cancer progression via JAK2/STAT3 phosphorylation-mediated cyclooxygenase-2 expression. *Genes Genomics*, 2020; 42, 127–33.
  40. Bhattacharya S, Dunn P, Thomas CG, et al. ImmPort, toward repurposing of open access immunological assay data for translational and clinical research. *Sci Data*, 2018; 5, 180015.
  41. Lin M, Zhang XL, You R, et al. Neoantigen landscape in metastatic nasopharyngeal carcinoma. *Theranostics*, 2021; 11, 6427–44.
  42. Wu JC, Zhao WY, Zhou BB, et al. TSNAdb: a database for tumor-specific neoantigens from immunogenomics data analysis. *Genomics Proteomics Bioinformatics*, 2018; 16, 276–82.
  43. Almeida LG, Sakabe NJ, deOliveira AR, et al. CTdatabase: a knowledge-base of high-throughput and curated data on cancer-testis antigens. *Nucleic Acids Res*, 2009; 37, D816–9.
  44. Zhou Y, Zhang YT, Lian XC, et al. Therapeutic target database update 2022: facilitating drug discovery with enriched comparative data of targeted agents. *Nucleic Acids Res*, 2022; 50, D1398–407.
  45. Southan C, Sharman JL, Benson HE, et al. The IUPHAR/BPS guide to PHARMACOLOGY in 2016: towards curated quantitative interactions between 1300 protein targets and 6000 ligands. *Nucleic Acids Res*, 2016; 44, D1054–68.
  46. Mullard A. 2017 FDA drug approvals. *Nat Rev Drug Discov*, 2018; 17, 81–5.
  47. Wang YZ, Wu WB, Zhu M, et al. Integrating expression-related SNPs into genome-wide gene- and pathway-based analyses identified novel lung cancer susceptibility genes. *Int J Cancer*, 2018; 142, 1602–10.
  48. Chen ZM, Yao NH, Zhang S, et al. Identification of critical radioresistance genes in esophageal squamous cell carcinoma by whole-exome sequencing. *Ann Transl Med*, 2020; 8, 998.
  49. Cui XY, Pei XS, Wang H, et al. ALG3 promotes peritoneal metastasis of ovarian cancer through increasing interaction of  $\alpha$ 1, 3-mannosylated uPAR and ADAM8. *Cells*, 2022; 11, 3141.

50. Sun XQ, He ZY, Guo L, et al. ALG3 contributes to stemness and radioresistance through regulating glycosylation of TGF- $\beta$  receptor II in breast cancer. *J Exp Clin Cancer Res*, 2021; 40, 149.
51. Ke SB, Qiu H, Chen JM, et al. ALG3 contributes to the malignancy of non-small cell lung cancer and is negatively regulated by MiR-98-5p. *Pathol Res Pract*, 2020; 216, 152761.
52. Chen JR, Huang MS, Lee YC, et al. Potential clinical value of 5-hydroxytryptamine receptor 3C as a prognostic biomarker for lung cancer. *J Oncol*, 2021; 2021, 1901191.
53. Zhou HY, Zhang CF, Li HR, et al. A novel risk score system of immune genes associated with prognosis in endometrial cancer. *Cancer Cell Int*, 2020; 20, 240.
54. Ma MW, Li J, Zhang ZM, et al. The role and mechanism of microRNA-1224 in human cancer. *Front Oncol*, 2022; 12, 858892.
55. Lacombe L, Hovington H, Brisson H, et al. UGT2B28 accelerates prostate cancer progression through stabilization of the endocytic adaptor protein HIP1 regulating AR and EGFR pathways. *Cancer Lett*, 2023; 553, 215994.
56. Henderson S, Chakravarthy A, Su XP, et al. APOBEC-mediated cytosine deamination links PIK3CA helical domain mutations to human papillomavirus-driven tumor development. *Cell Rep*, 2014; 7, 1833–41.
57. Roberts SA, Lawrence MS, Klimczak LJ, et al. An APOBEC cytidine deaminase mutagenesis pattern is widespread in human cancers. *Nat Genet*, 2013; 45, 970–6.
58. Tanaka M, Koyama T, Sakurai T, et al. The endothelial adrenomedullin-RAMP2 system regulates vascular integrity and suppresses tumour metastasis. *Cardiovasc Res*, 2016; 111, 398–409.
59. de Paula Souza DPS, Dos Reis Pereira Queiroz L, de Souza MG, et al. Identification of potential biomarkers and survival analysis for oral squamous cell carcinoma: a transcriptomic study. *Oral Dis*, 2023; 29, 2658–66.
60. Li J, Zhou L, Jiang HY, et al. Inhibition of FOSL2 aggravates the apoptosis of ovarian cancer cells by promoting the formation of inflammasomes. *Genes Genomics*, 2022; 44, 29–38.
61. Xu P, Wang L, Xie X, et al. Hsa\_circ\_0001869 promotes NSCLC progression via sponging miR-638 and enhancing FOSL2 expression. *Aging (Albany NY)*, 2020; 12, 23836–48.
62. Wan XY, Guan SD, Hou YX, et al. FOSL2 promotes VEGF-independent angiogenesis by transcriptionally activating Wnt5a in breast cancer-associated fibroblasts. *Theranostics*, 2021; 11, 4975–91.
63. Neefjes J, Jongsma MLM, Paul P, et al. Towards a systems understanding of MHC class I and MHC class II antigen presentation. *Nat Rev Immunol*, 2011; 11, 823–36.
64. Kaur S, Rajoria P, Chopra M. HDAC6: a unique HDAC family member as a cancer target. *Cell Oncol (Dordr)*, 2022; 45, 779–829.
65. Liu G, Zhao H, Song Q, et al. Long non-coding RNA DPP10-AS1 exerts anti-tumor effects on colon cancer via the upregulation of ADCY1 by regulating microRNA-127-3p. *Aging (Albany NY)*, 2021; 13, 9748–65.
66. El-Zein M, Cheishvili D, Gotlieb W, et al. Genome-wide DNA methylation profiling identifies two novel genes in cervical neoplasia. *Int J Cancer*, 2020; 147, 1264–74.